Prompt γ spectroscopic studies of fragment nuclei in thermal neutron induced fission of ^{235}U

S. Mukhopadhyay,[1] L. S. Danu,[1] D. C. Biswas,[1,*] A. Goswami,[2] P. N. Prashanth,[1] L. A. Kinage,[1] A. Chatterjee,[1] and R. K. Choudhury[1]

[1]*Nuclear Physics Division, Bhabha Atomic Research Centre, Mumbai 400085, India*

[2]*Radio Chemistry Division, Bhabha Atomic Research Centre, Mumbai 400085, India*

(Received 17 January 2012; revised manuscript received 9 May 2012; published 22 June 2012)

The prompt γ-γ coincidence technique has been used to carry out the spectroscopic study of the level schemes and to derive the relative isotopic yield distributions of fission fragment nuclei employing the ^{235}U(n_{th}, f) reaction for the first time. From the coincidence rates of various Ba isotopes with ^{90}Kr nucleus and of Sr isotopes with ^{138}Xe nucleus, it has been found that either the 2n or 3n neutron evaporation channels dominate during the fission process. The average angular momenta for three complementary pairs have been estimated. The yrast and near-yrast level structures in several isotopes of six elements (Sr, Xe, Kr, Ba, Zr, and Te) have been deduced. The level schemes obtained are compared with earlier reported works, where different reactions or spontaneous fission (SF) data were used.

DOI: 10.1103/PhysRevC.85.064321 PACS number(s): 25.85.Ec, 24.75.+i, 23.20.Lv, 27.90.+b

I. INTRODUCTION

Nuclear fission involves a large-scale collective rearrangement of nuclear matter in a short time scale. The shape evolution of a fissioning nucleus is directly related to the fission fragment mass distribution. Various theoretical models have already been put forward to describe the complex shape evolution of deformed nuclei [1–5]. It has been observed that the nuclear shell closures have a strong influence on the fission fragment mass distribution [6]. A new fission mode was reported earlier from the fragment mass measurement [7], but the results remain ambiguous [8]. All these facts point towards critical aspects of the fission process which require a detailed understanding by measuring various experimental observables with improved experimental techniques.

There are several methods of measuring the relative isotopic yield distribution of fission fragment nuclei [9]. Yield distributions of light fission fragments ($A = 76$ to $A = 115$) from thermal neutron induced fission of various fissioning systems have been determined using the Lohengrin mass separator [10,11], providing valuable insight into the fission process. Recently, a new experimental setup based on γ spectrometry coupled with Lohengrin was used for measuring both light and heavy fragments in the ^{239}Pu($n_{\rm th}$, f) reaction [12]. In that measurement, the fission products were implanted in a tape located inside a vacuum chamber, placed at the focal point of the spectrometer. The prompt γ-γ coincidence technique was successfully used in measuring the relative isotopic yield distribution of fragment nuclei in the spontaneous fission of ^{248}Cm and ^{252}Cf [7,13,14]. Using this technique, it is possible to identify the individual fission fragments from the coincidence relationship of two emitted prompt γ rays. However, this method has not been exploited for the thermal neutron induced fission of ^{235}U.

Along with the relative isotopic yield distribution measurement of fission fragment nuclei, the scope of studying the level structures of individual neutron-rich fragment nuclei using fission reaction is unique and substantial. Spectroscopic studies of level structures of such neutron-rich nuclei continue to enrich our knowledge on the evolution of nuclear shell structure. These nuclei, with a higher neutron-to-proton ratio are not always easily accessible by conventional fusion evaporation reactions, which are best suited for high-spin studies. One of the ways to produce and carry out a level structure investigation of these nuclei is the fission process, which may be spontaneous or induced by a projectile. Much work has already been done on these sets of nuclei by means of the spontaneous fission of ^{252}Cf [15–17] and ^{248}Cm [14,18–20] sources, heavy-ion induced fusion-fission reactions [6,21,22] and also using deep-inelastic reactions [23,24]. It is desirable to extend these measurements to the thermal neutron induced fission of ^{235}U as well to investigate those nuclei whose population in the above-mentioned reactions are low [25]. The data will also be useful to obtain level structure information of the nuclei with comparable population out of all these fissioning systems to compare the results for an unambiguous conclusion. Another interesting common area of investigation is to understand the population of high-spin states in fission fragment nuclei, which depends on the fissioning system as well as on the mass of the fragment nucleus. This might shed light on the mechanisms of the generation of fragment spin from a fissioning nucleus having zero or a few units of angular momentum.

In the present work, we report the relative isotopic yield distribution of the isotopes, produced in thermal neutron induced fission of ^{235}U, using the prompt γ-γ coincidence measurement technique. The coincidence rates for four Ba and three Sr isotopes with ^{90}Kr and ^{138}Xe, respectively, have also been measured, which directly provide information on the number of neutron emissions from the correlated fragment pairs. An attempt has been made to estimate the mean fragment spins of the complementary pairs from their intra-ground-band cascade intensity ratios. Also, the systematic study of yrast and near-yrast level structures of the neutron-rich fission fragment nuclei has been presented.

*dcbiswas@barc.gov.in

II. EXPERIMENTAL PROCEDURE

The experiment was performed at the Canada India Research Utility Services (CIRUS) reactor facility, Bhabha Atomic Research Center (BARC), Mumbai. A schematic diagram depicting the geometry of the setup is shown in Fig. 1. The details of this experimental setup were reported earlier by Biswas *et al.* [26]. The shielding arrangement was made in such a manner so that a collimated radial neutron beam of ∼10-mm diameter impinges on the target. The target was uranium aluminide (UAl_3, with 17% ^{235}U enrichment) in pellet form, with a material density of ∼5.1 gm/cm^3. The 3-mm thick target, fully sealed in a Teflon disk-type capsule, was bombarded by the thermal neutrons from the reactor. The thickness of the Teflon, covering the front face of the target, was measured as 1 mm, whereas the Teflon thickness in the rear (base of the target material) was 5 mm. The neutron flux at the target position was $\sim 4 \times 10^7$ cm^{-2} s^{-1}. Deexciting γ rays from the fission fragment nuclei were detected by two clover germanium detectors in coincidence mode, mounted in a vertical ring-type structure with $\phi = 72^\circ$. The clover detectors were mounted at a distance of 24 cm from the target along with their anti-Compton shields. The Compton suppressed list-mode data were collected with the condition of firing by both the detectors in a single event. A total of $3 \times 10^6 \gamma$-γ coincident events were recorded for further offline analysis.

III. DATA ANALYSIS

In the offline analysis of the experimental data the RADWARE software package [27,28] was used. The acquired data, after presorting (i.e., after performing the energy calibration followed by the software gain matching over the entire range of energy), were sorted into conventional γ-γ matrices. Different time windows were selected to reduce random coincidence events, including the general reactor background. The matrices were then used to determine the correlation between two coincident γ rays, which helped in building the level schemes of the complementary heavy and light fission fragments.

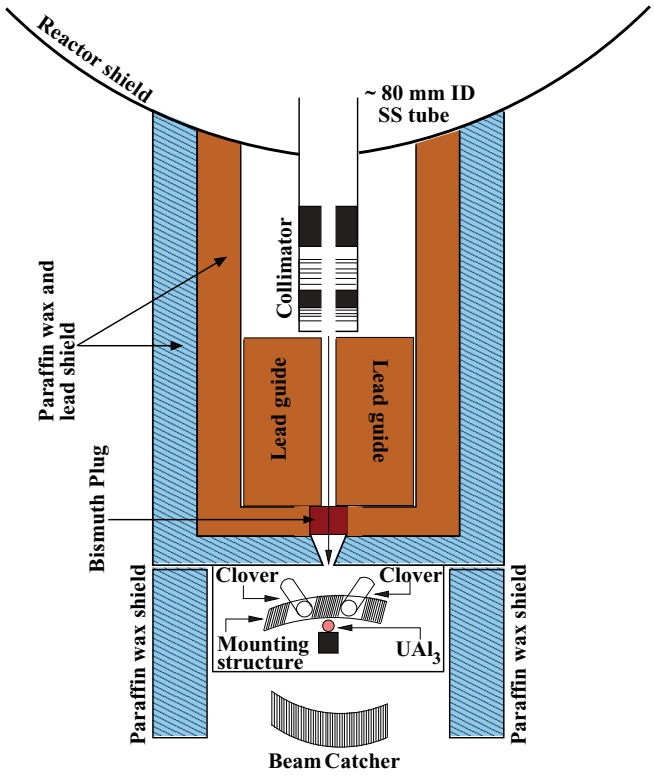

FIG. 1. (Color online) Schematic diagram of the experimental setup at the CIRUS reactor facility.

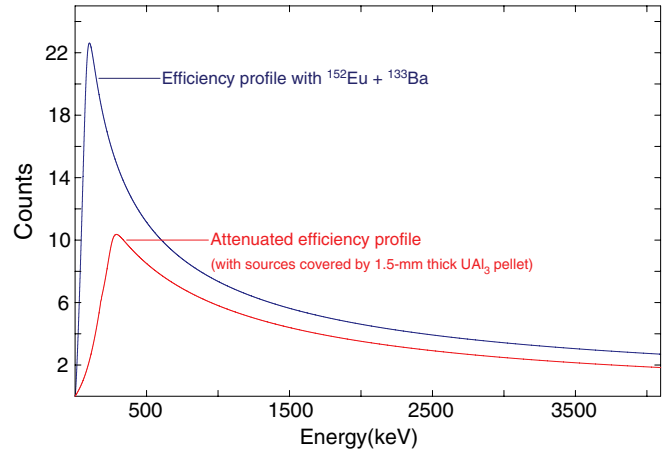

FIG. 2. (Color online) Efficiency profiles as derived and subsequently used in the present analysis to deduce relative intensities.

To extract the relative yield distribution by measuring the intensities of the γ rays, the interplay between the neutron and γ absorption in the thick target needs to be considered. It was deduced that the neutron absorption, or in other words the rate of reaction, remains almost uniform throughout the thickness of the target. To estimate the self-absorption of the γ energies in the thick target, data were taken by placing the calibration sources (^{152}Eu, ^{133}Ba) just beneath an identically sealed, half-thick (1.5 mm) UAl_3 target. Another set of data were taken (for the same time period) to check for the absorption of the γ rays from the sources in the thick Teflon base. The γ-detection efficiency profile was then ultimately derived out of these two data sets (Fig. 2). It has been calculated that, due to the combined effect of neutron and gamma absorption in the target, the present estimation of γ-ray intensities using the derived efficiency profile can lead to an uncertainty of ∼25% for γ rays of 150 keV. For γ rays of above 200-keV energy this error is less than 10%.

IV. RELATIVE ISOTOPIC YIELD DISTRIBUTION AND COINCIDENCE RATES

The profile of the relative isotopic yield distribution provides information about the distribution of the relative yields of several isotopes of an element for a fixed charge split in a fissioning system. The isotopic yield distribution is normally assumed to be Gaussian, defined by its most probable mass (A_p) and the width parameter (σ_A) [29]. The most probable mass for a particular Z is expected to be governed by the mass-to-charge ratio (A_F/Z_F) of the fissioning nucleus, and the relative isotopic yield distribution around this most probable mass follows a Gaussian profile.

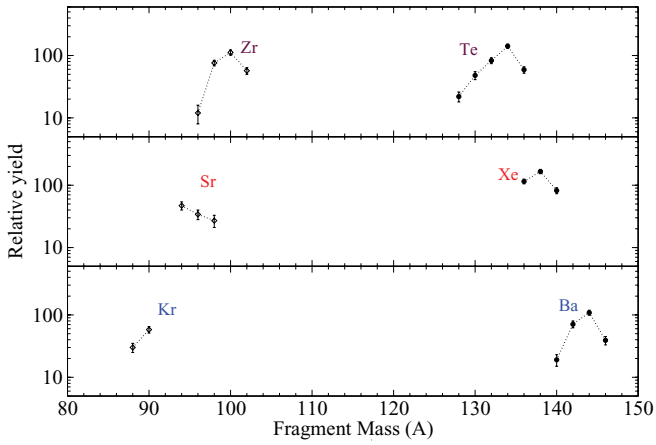

FIG. 3. (Color online) Yield distribution of fragment partners as obtained from thermal neutron induced fission of ^{235}U.

In the present work, the relative isotopic yield distributions of several even-even isotopes of the complementary charge pairs, viz., (Kr–Ba), (Sr–Xe), and (Zr–Te) have been obtained (Fig. 3). For each isotope of a particular Z, the relative yield was estimated from the intensity of the $2^+ \rightarrow 0^+$ transition when a gate was put on the $4^+ \rightarrow 2^+$ transition. In instances where more than one transition was seen feeding the 2^+ state (viz., ^{96}Sr, ^{98}Zr), the individual gated spectra (with gates on the feeding transitions) were added to form one single spectrum. The relative yield of that isotope was then determined by measuring the intensity of the $2^+ \rightarrow 0^+$ transition from that single spectrum, followed by a correction due to the detection efficiency of the detectors. The transition(s) which was (were) used as gate(s) and the $2^+ \rightarrow 0^+$ transition for each isotope is (are) given in Table I.

For the Zr–Te pair, the relative isotopic yield distributions fairly represents a Gaussian shape. For the other two charge pairs, namely, Sr–Xe and Kr–Ba, the data were not sufficient to get a reasonable shape of the distribution (Fig. 3). To get an estimate of the relative isotopic yield distribution parameters for a fixed charge split, the mass numbers (A') of the isotopes after the necessary neutron number corrections were plotted on the same abscissa. These are shown in the upper panels of Fig. 4. The data points were then fitted by a pure Gaussian function to obtain the parameters. In panel (I) of Fig. 4, the data points at $A = 128$ and $A = 130$ ($A' = 128.3$ and 130.3, respectively, after the neutron number corrections), which deviate from the overall Gaussian distribution, were omitted while fitting. The enhanced yield for $A' = 128.3$, 130.3 [in panel (I)] may be due to the additional contribution from their precursors' β decay that populates the 4^+ state of the daughter nucleus, which then comes to the ground state by the subsequent emission of two coincident ($4^+ \rightarrow 2^+$ and $2^+ \rightarrow 0^+$) γ rays of comparable strength. It is to be noted that the contribution from the precursors through subsequent β decay is expected to be significant for those fission fragment nuclei which are close to the β-stability line (viz. ^{128}Te, ^{130}Te), and having a low fission yield. In the lower panels of Fig. 4, the corresponding data from the literature [29] for the same two complementary charge pairs are plotted and fitted in a similar way. The extracted parameters out of these fittings have been tabulated in Table II. It is evident from the values of the parameters that there is reasonable agreement between the present data set and the data from the literature [29].

TABLE I. The details of the gating transition(s) and the $2^+ \rightarrow 0^+$ transition, the intensity of which was measured while determining the relative isotopic yield distribution.

Isotope	Gating transition(s) (keV)	Measured transition ($2^+ \rightarrow 0^+$) (keV)
^{94}Sr	1309, 1089	837
^{96}Sr	978, 692, 1161	815
^{98}Sr	289	144
^{136}Xe	381	1313
^{138}Xe	484, 875	589
^{140}Xe	458	377
^{88}Kr	869	775
^{90}Kr	1123, 799, 656	707
^{140}Ba	528	602
^{142}Ba	475	359
^{144}Ba	331	199
^{146}Ba	333	181
^{96}Zr	1107	1750
^{98}Zr	825, 620, 583	1223
^{100}Zr	352	213
^{102}Zr	327	152
^{128}Te	754	743
^{130}Te	794	840
^{132}Te	696	974
^{134}Te	297	1279
^{136}Te	424	606

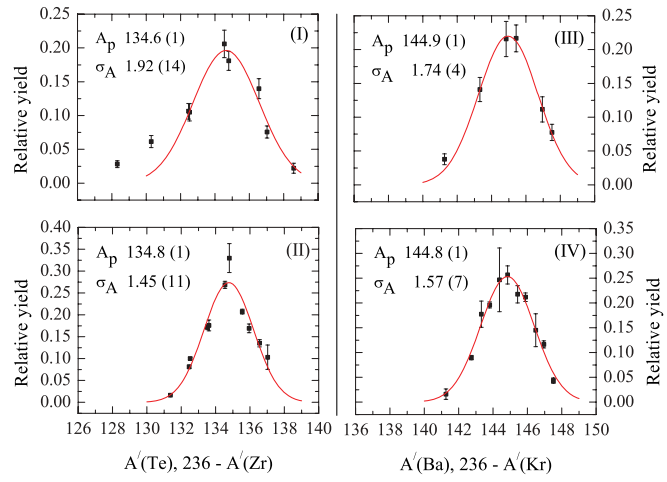

FIG. 4. (Color online) Upper panels: Relative isotopic yield distribution for complementary elements from the present measurement, fitted by a Gaussian function. Lower panels: Corresponding data for the same complementary elements from the literature [29], fitted by a Gaussian function. (I) and (II): Complementary elements: Zr–Te; (III) and (IV): Complementary elements: Kr–Ba.

TABLE II. Relative isotopic yield distribution parameters, as obtained from the present data set and the data from the literature.

	A_p (Present work)	A_p (Ref. [29])	σ_A (Present work)	σ_A (Ref. [29])
Zr–Te	134.6(1)	134.8(1)	1.92(14)	1.45(11)
Kr–Ba	144.9(1)	144.8(1)	1.74(4)	1.57(7)

Along with the relative isotopic yield distribution of an element, coincidence rates of various Ba and Sr isotopes (with ^{90}Kr and ^{138}Xe nucleus, respectively) were also measured from the present data set. In Fig. 5, the lower panel shows the coincidence rates of three Sr isotopes with ^{138}Xe nucleus, wherein, the upper panel depicts the same for the four Ba isotopes with ^{90}Kr nucleus, as produced in the thermal neutron induced fission of ^{235}U. When gates were pulled on the lower-lying strong transitions of ^{138}Xe, we clearly observed the strong γ rays of ^{94}Sr($4n$), ^{95}Sr($3n$), and ^{96}Sr($2n$) in addition to the transitions in ^{138}Xe (Fig. 6). Hence, for the Sr isotopes, the rates were deduced by measuring the relative intensities of their first excited state to ground state transitions from a single spectrum [sum spectrum with individual gates on (483 keV, $4^+ \rightarrow 2^+$ transition) and (589 keV, $2^+ \rightarrow 0^+$ transition)] of ^{138}Xe. The final numbers were corrected, of course, by the γ-detection efficiency of the detectors. Similarly, when a gate

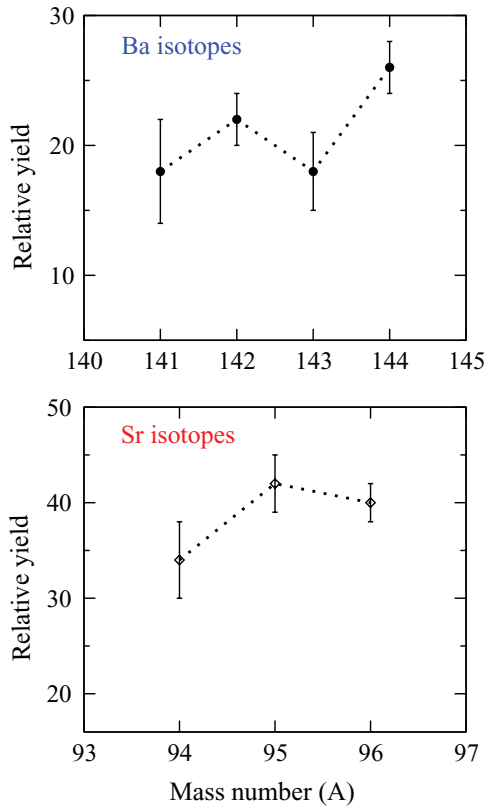

FIG. 5. (Color online) Upper panel: Rates of Ba isotopes in coincidence with the ^{90}Kr nucleus as produced in the thermal neutron induced fission of ^{235}U. Lower panel: Rates of Sr isotopes in coincidence with the ^{138}Xe nucleus as produced in the thermal neutron induced fission of ^{235}U.

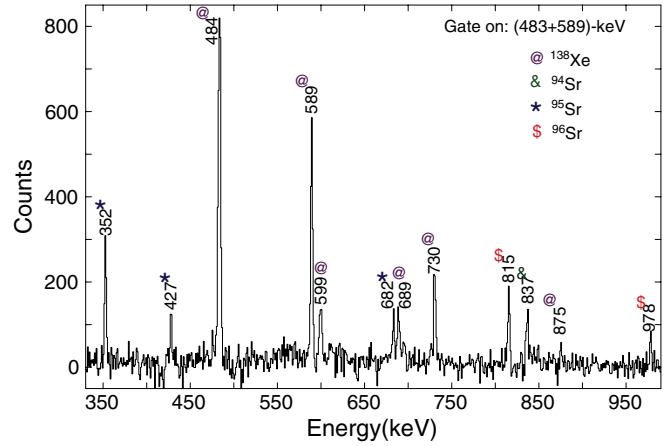

FIG. 6. (Color online) Representative gated spectrum of ^{138}Xe. Almost all the clean peaks that come from ^{138}Xe and its complementary fragments ($^{94-96}$Sr) have been labeled.

was set on the 707 keV ($2^+ \rightarrow 0^+$) transition of ^{90}Kr, the strong γ lines of ^{142}Ba ($4n$), ^{143}Ba ($3n$), and ^{144}Ba ($2n$) were very much evident (Fig. 7). So, while obtaining the rates for the Ba isotopes, this single spectrum, gated on the 707-keV transition of ^{90}Kr, was used. It is evident from Fig. 5 that in the case of Xe–Sr fragment pair production, the $3n$ neutron evaporation channel dominates among others, whereas, in the case of Ba–Kr fragment pairs, the $2n$ neutron evaporation channel has the maximum yield.

V. ANGULAR MOMENTUM OF PRIMARY FISSION PRODUCTS

The angular momentum distribution of fission products provides information on the neck vibration at the scission point and is an important fission observable. There are several methods to estimate fragment angular momentum, which are essentially based on various types of information related to γ-ray deexcitation, for example, (a) the angular distribution of

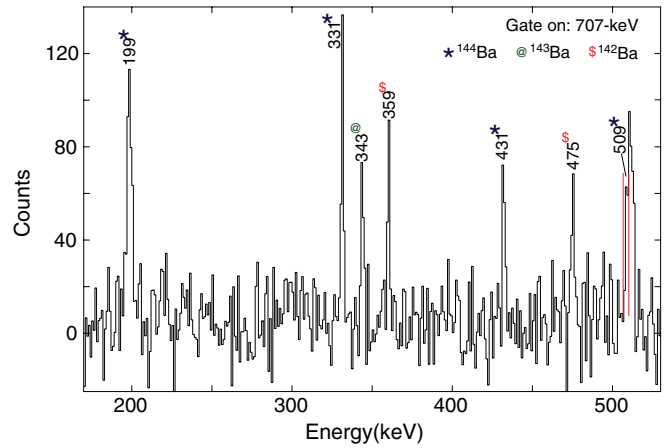

FIG. 7. (Color online) Representative gated spectrum of ^{90}Kr. The existence of the 509-keV transition ($8^+ \rightarrow 6^+$) in ^{144}Ba is also evident in the spectrum and it is located in the region between the two vertical red lines.

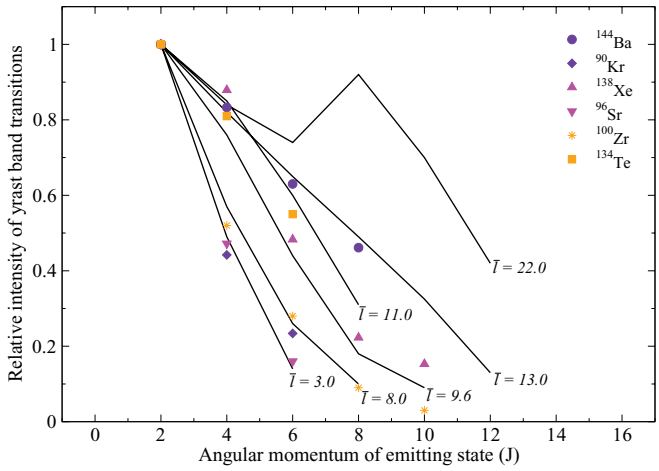

FIG. 8. (Color online) Comparison of the observed relative intra-ground-state-band transition intensities from the present data with those observed in various (charged particle, xn) reactions (solid lines). The reaction data are labeled with the average angular momentum of the reaction as calculated from optical model codes.

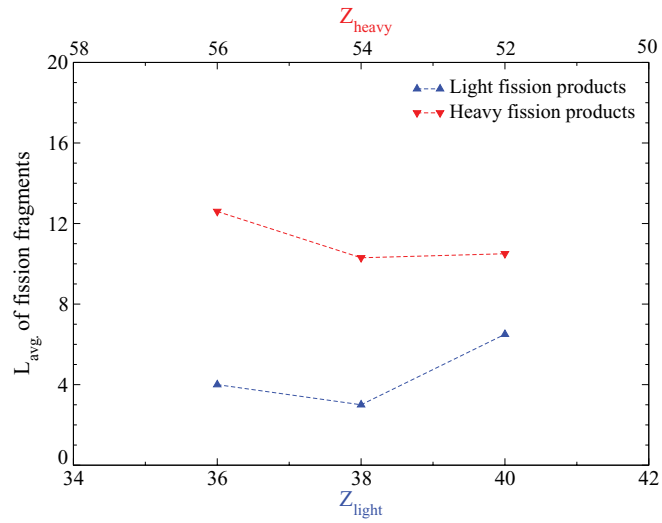

FIG. 9. (Color online) Plot of the derived mean angular momentum as a function of atomic number. Uncertainties of 1 to 2$\hbar$ have to be considered.

the gross unresolved prompt γ rays from fission; (b) studies of γ-ray multiplicities and total energy in fission; (c) isomeric yield measurements; and (d) the measurement of the relative intensities of the intraband prompt γ transition in even-even fission products.

In the present work, the relative intensities of the prompt transitions which depopulate the yrast levels of the ground state bands were used to estimate the mean fragment angular momentum for six even-even fission products, viz., ^{144}Ba, ^{90}Kr, ^{138}Xe, ^{96}Sr, ^{134}Te, and ^{100}Zr. The procedure described in Ref. [30] was followed. The experimental data on the relative intensities of the ground state bands of these nuclei have been plotted on the canvas of Fig. 6 in Ref. [30]. To compare the relative intensity profiles of the higher-lying transitions of these fragment nuclei to those of the nuclei from specific reactions (Table II in Ref. [30]), the relative intensities of the $2^+ \rightarrow 0^+$ transitions have been normalized to unity. It is obvious from Figs. 8 and 6 in Ref. [30] that the mean angular momenta of the fragments are comparable to those estimated from ^{252}Cf data. A liner interpolation of the experimental intensities for ^{144}Ba gives an l_{avg} value of $\sim$12.8. Following a similar interpolation method, the l_{avg} values for other isotopes have been extracted (Table III) and plotted in Fig. 9. Although there remains an uncertainty of 1 to 2$\hbar$ due to the difficulties associated with the present method [30], the mechanism of generation of such high l_{avg} from a fissioning system with low l_{avg} still remains an interesting subject for future studies.

In Fig. 9, it is interesting to note that the average angular momenta for the fission fragments distinctly fall into two groups. The light fragments tend to have a lower l_{avg} than those of the heavier fragments. Also, the angular momenta for the heavier and lighter complementary fragments appear to approach each other as the symmetric division is approached.

TABLE III. Average angular momentum of fission fragment nuclei, as obtained from the present data set. Uncertainties of 1 to 2$\hbar$ need to be taken into account for the derived numbers.

^{90}Kr	^{96}Sr	^{100}Zr	^{134}Te	^{138}Xe	^{144}Ba
$\sim 4\hbar$	$\sim 3\hbar$	$\sim 6.5\hbar$	$\sim 10.5\hbar$	$\sim 10.3\hbar$	$\sim 12.8\hbar$

VI. RESULTS OBTAINED FROM COINCIDENCE ANALYSIS

A. Sr and its complementary fragment Xe

In the thermal neutron induced fission of ^{235}U, Sr isotopes are the complementary fragments of Xe isotopes centered around ^{138}Xe (Fig. 3). The latest work on ^{95}Sr was reported by Hwang *et al.* [31]. We could see the γ lines clearly up to $I = (\frac{13}{2}^+)\hbar$ ($E_x = 2.344$ MeV) (Fig. 10) even in the gated spectrum of its complementary fragment, thus confirming the previous assignment of the levels. Similar to Hwang *et al.* [31], we also did not see the 886.1-keV transition between 1238.5- and 352.0-keV states as seen in the β^- decay from the $5/2^-$ state of ^{95}Rb [32]. This observation, together with the logic provided by Hwang *et al.* [31], supports the spin and parity assignment to the 1238.5-keV level. The relative intensities of the observed transitions have been compared with the previous spontaneous fission (SF) data [31] in Table IV.

In the present data set ^{96}Sr happens to be one of the well-populated nucleus among the Sr isotopes. The latest work done on this nucleus has been reported by Rząca-Urban *et al.* [33]. In our data, we could see transitions up to $I = 9^-\hbar$ ($E_x = 3.524$ MeV) (Fig. 10). Similar to the ^{248}Cm data [34], we did not see the excited 0^+ levels at 1229 keV (although included in the level scheme to assist the visualization of its probable placement) and 1465 keV. Although we could see the quasirotational structure built on a possible 0_2^+ excitation, the proposed deformed band with the 0_3^+ level at 1465 keV as bandhead remains elusive like all other previous experimental investigations. Therefore, the

TABLE IV. Relative intensities of the γ rays in the fission fragment nuclei as derived in the present measurement. The intensity errors range from 5% for the strong transitions to 25% for the weak transitions. The earlier reported numbers have been normalized to the highest observed intensity for each nucleus in the present measurement.

E_x (MeV)	E_γ (MeV)	$J_i^\pi \rightarrow J_f^\pi$	*Relative Intensity* (present work)	*Relative Intensity* (earlier work)
^{90}Kr				
0.707	0.707	$2^+ \rightarrow 0^+$	>226.4	–
1.363	0.656	$2^+ \rightarrow 2^+$	52.9	–
	1.363	$2^+ \rightarrow 0^+$	62.5	–
1.506	0.799	$3^- \rightarrow 2^+$	73.5	–
1.765	0.402	$4^+ \rightarrow 2^+$	47.1	–
1.830	1.123	$4 \rightarrow 2^+$	100	–
2.852	1.022		52.9	–
3.895	1.043		47.0	–
^{94}Sr				(from Ref. [33])
0.837	0.837	$2^+ \rightarrow 0^+$	>193	–
1.926	1.089	$3^{(-)} \rightarrow 2^+$	93.0	82.8(2.8)
2.146	1.309	$4^+ \rightarrow 2^+$	100	100(5.7)
2.604	0.678	$4^- \rightarrow 3^{(-)}$	27.9	42.8(2.8)
3.156	1.010	$6^+ \rightarrow 4^+$	41.9	34.3(2.8)
3.923	0.767	$7^- \rightarrow 6^+$	34.9	28.0(1.7)
^{95}Sr				(from Ref. [31])
0.352	0.352	$(\frac{3}{2}^+) \rightarrow \frac{1}{2}^+$	>100	–
0.556	0.204	$(\frac{7}{2}^+) \rightarrow (\frac{3}{2}^+)$	100	100
1.238	0.682	$(\frac{9}{2}^+) \rightarrow (\frac{7}{2}^+)$	32.7	59.2
1.665	0.427	$(\frac{11}{2}^+) \rightarrow (\frac{9}{2}^+)$	19.1	45.4
2.344	0.679	$(\frac{13}{2}^+) \rightarrow (\frac{11}{2}^+)$	8.8	10.9
^{96}Sr				(from Ref. [34])
0.815	0.815	$2^+ \rightarrow 0^+$	>100	–
1.793	0.978	$4^+ \rightarrow 2^+$	100	100(7.5)
2.786	0.993	$6^+ \rightarrow 4^+$	33.8	20(2.5)
2.467	0.674	$6^+ \rightarrow 4^+$	53.1	42.5(2.5)
3.126	0.659	$8^+ \rightarrow 6^+$	43.7	50(2.5)
3.524	0.398	$9^- \rightarrow 8^+$	50.7	22.5(2.5)
^{98}Zr				(from Ref. [34])
1.223	1.223	$2^+ \rightarrow 0^+$	>220	–
2.048	0.825	$4^+ \rightarrow 2^+$	55.0	8.6(1.7)
1.806	0.583	$3^- \rightarrow 2^+$	65.0	53.4(3.4)
1.843	0.620	$4^+ \rightarrow 2^+$	100	100(5.2)
2.490	0.647	$6^+ \rightarrow 4^+$	70.0	62.1(3.4)
3.215	0.725	$8^+ \rightarrow 6^+$	35.0	29.3(3.4)
3.984	0.769	$(10^+) \rightarrow 8^+$	23.1	13.8(5.2)
3.064	1.221		22.6	5.2(1.7)
^{100}Zr				(from Ref. [47])
0.213	0.213	$2^+ \rightarrow 0^+$	>100	–
0.564	0.352	$4^+ \rightarrow 2^+$	100	100
1.062	0.498	$6^+ \rightarrow 4^+$	62.1	77.4
1.687	0.625	$8^+ \rightarrow 6^+$	17.0	30.9
2.426	0.739	$10^+ \rightarrow 8^+$	9.6	6.2
^{102}Zr				(from Ref. [50])
0.152	0.152	$2^+ \rightarrow 0^+$	>100	–
0.478	0.327	$4^+ \rightarrow 2^+$	100	100
0.965	0.487	$6^+ \rightarrow 4^+$	48.2	63.8
1.661	1.183	$5^- \rightarrow 4^+$	53.9	1.0

TABLE IV. (*Continued*.)

E_x (MeV)	E_γ (MeV)	$J_i^\pi \rightarrow J_f^\pi$	*Relative Intensity* (present work)	*Relative Intensity* (earlier work)	
2.092	0.431	$7^- \rightarrow 5^-$	25.5	4.8	
^{128}Te				(from Ref. [24])	
0.743	0.743	$2^+ \rightarrow 0^+$	>100	157	
1.497	0.754	$4^+ \rightarrow 2^+$	100	100	
1.811	0.314	$6^+ \rightarrow 4^+$	62.5	46	
^{130}Te				(from Ref. [24])	
0.840	0.840	$2^+ \rightarrow 0^+$	>100	531	
1.634	0.794	$4^+ \rightarrow 2^+$	100	100	
1.816	0.182	$6^+ \rightarrow 4^+$	45.9	10.7	
2.147	0.331	$7^- \rightarrow 6^+$	22.9	1.2	
^{134}Te				(from Ref. [49])	
1.279	1.279	$2^+ \rightarrow 0^+$	>100	113.1	
1.576	0.297	$4^+ \rightarrow 2^+$	100	100	
1.691	0.115	$6^+ \rightarrow 4^+$	65.0	22.2	
2.397	0.706	$6^+ \rightarrow 6^+$	15.8	10.4	
2.727	0.330	$5^+ \rightarrow 6^+$	10.0	3.7	
^{136}Te				(from Ref. [51])	
0.606	0.606	$2^+ \rightarrow 0^+$	>100	106.4	
1.030	0.424	$4^+ \rightarrow 2^+$	100	100(10.6)	
1.382	0.352	$6^+ \rightarrow 4^+$	72.7	84(2)	
2.132	0.750	$8^+ \rightarrow 6^+$	46.3	39.4(4.2)	
2.792	0.660	$10^+ \rightarrow 8^+$	28.2	20.2(2.1)	
^{136}Xe					
1.313	1.313	$2^+ \rightarrow 0^+$	>100	–	
1.694	0.381	$4^+ \rightarrow 2^+$	100	–	
1.891	0.197	$6^+ \rightarrow 4^+$	73.3	–	
^{137}Xe				(from Ref. [52])	
1.220	1.220	$\frac{11}{2}^- \rightarrow \frac{7}{2}^-$	>100	115	
1.620	0.400	$\frac{15}{2}^- \rightarrow \frac{11}{2}^-$	100	100	
1.934	0.314	$\frac{19}{2}^- \rightarrow \frac{15}{2}^-$	76.9	72.4	
2.980	1.046	$\frac{23}{2}^- \rightarrow \frac{19}{2}^-$		24.1	
^{138}Xe				(from NNDC)[a]	
0.589	0.589	$2^+ \rightarrow 0^+$	>116.2	92.7(1.0)	
1.072	0.484	$4^+ \rightarrow 2^+$	100	} 167.0(1.0)	
1.556	0.483	$6^+ \rightarrow 4^+$	54.9		
2.285	0.730	$8^+ \rightarrow 6^+$	25.4	32.5(1.0)	
2.973	0.688	$10^+ \rightarrow 8^+$	17.4	26.2(1.0)	
3.572	0.599	$12^+ \rightarrow 10^+$	9.1	18.4(5.6)	
1.464	0.875	$(2^+) \rightarrow 2^+$	16.2	–	
^{139}Xe				(from NNDC)[a]	
0.594	0.571	$\frac{11}{2}^- \rightarrow \frac{7}{2}^-$	>100	133.3(6.7)	
1.179	0.585	$\frac{15}{2}^- \rightarrow \frac{11}{2}^-$	100	100(6.7)	
1.810	0.630	$\frac{19}{2}^- \rightarrow \frac{15}{2}^-$	46.7	46.6(4)	
^{140}Xe				(from NNDC)[a]	
0.377	0.377	$2^+ \rightarrow 0^+$	>100	115[^{252}Cf]	–
0.835	0.458	$4^+ \rightarrow 2^+$	100	100[^{252}Cf]	100[^{248}Cm]
1.417	0.582	$6^+ \rightarrow 4^+$	59.1	67.8[^{252}Cf]	60.9[^{248}Cm]
1.984	0.567	$8^+ \rightarrow 6^+$	41.9	48.3[^{252}Cf]	37.9[^{248}Cm]
2.591	0.607	$10^+ \rightarrow 8^+$	26.8	20.7[^{252}Cf]	18.4[^{248}Cm]
3.270	0.679	$12^+ \rightarrow 10^+$	20.7	12.6[^{252}Cf]	10.3[^{248}Cm]

TABLE IV. (*Continued.*)

E_x (MeV)	E_γ (MeV)	$J_i^\pi \rightarrow J_f^\pi$	*Relative Intensity* (present work)	*Relative Intensity* (earlier work)
^{142}Ba				(from Ref. [14])
0.359	0.359	$2^+ \rightarrow 0^+$	>100	117.6(5.9)
0.834	0.475	$4^+ \rightarrow 2^+$	100	100(5.9)
1.465	0.631	$6^+ \rightarrow 4^+$	59.7	47.1(3.5)
2.158	0.693	$8^+ \rightarrow 6^+$	31.4	15.3(2.4)
2.926	0.768	$10^+ \rightarrow 8^+$	25.2	2.7(0.4)
1.952	0.487	$7^- \rightarrow 6^+$	16.7	21.2(2.4)
^{143}Ba				(from NNDC)[a]
0.118	0.118	$\frac{9}{2}^- \rightarrow \frac{5}{2}^-$		8.1
0.461	0.343	$\frac{13}{2}^- \rightarrow \frac{9}{2}^-$	>100	161.3
0.954	0.493	$\frac{17}{2}^- \rightarrow \frac{13}{2}^-$	100	100
1.580	0.626	$\frac{21}{2}^- \rightarrow \frac{17}{2}^-$	47.5	32.3
1.525	0.571	$\frac{17}{2}^+ \rightarrow \frac{17}{2}^-$	39.1	1.6
1.411	0.457	$\frac{19}{2}^+ \rightarrow \frac{17}{2}^-$	52.6	30.6
1.880	0.300	$\frac{23}{2}^+ \rightarrow \frac{21}{2}^-$	31.7	21.0
	0.469	$\frac{23}{2}^+ \rightarrow \frac{19}{2}^+$	44.7	18.5
^{144}Ba				(from Ref. [14])
0.199	0.199	$2^+ \rightarrow 0^+$	>100	105.3(5.3)
0.530	0.331	$4^+ \rightarrow 2^+$	100	100(5.3)
0.961	0.431	$6^+ \rightarrow 4^+$	73.7	88.4(5.3)
1.470	0.509	$8^+ \rightarrow 6^+$	55.3	47.4(5.3)
2.043	0.573	$10^+ \rightarrow 8^+$	11.7	12.6(1.1)
1.355	0.394	$7^- \rightarrow 6^+$	17.3	25.3(2.1)
1.772	0.417	$9^- \rightarrow 7^-$	12.7	14.7(1.1)
	0.302	$9^- \rightarrow 8^+$	16.0	24.2(2.1)
2.278	0.506	$11^- \rightarrow 9^-$	21.5	20.0(2.1)

[a]National Nuclear Data Center (NNDC), http://www.nndc.bnl.gov/

existence of 0_2^+ and 0_3^+ levels remains doubtful. In our present data set, we confirm most of the low-spin levels observed in β^- decay [35], but we do not see the levels at 1628 and 2150 keV. It is to be noted that in another recent work [36] where the ^{238}U(α, f) fusion-fission reaction was employed to study this nucleus, the 3.524-MeV level ($I = 9^-$) and the feeding

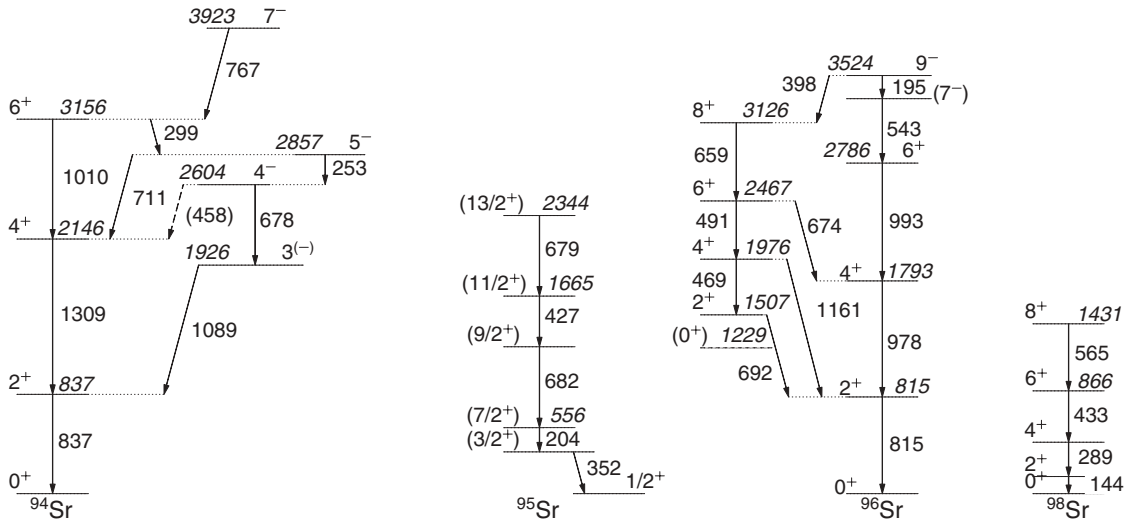

FIG. 10. Partial level schemes of Sr isotopes, as deduced from the present data set following coincidence analysis. The spins and parities of the levels have been adopted from earlier published works.

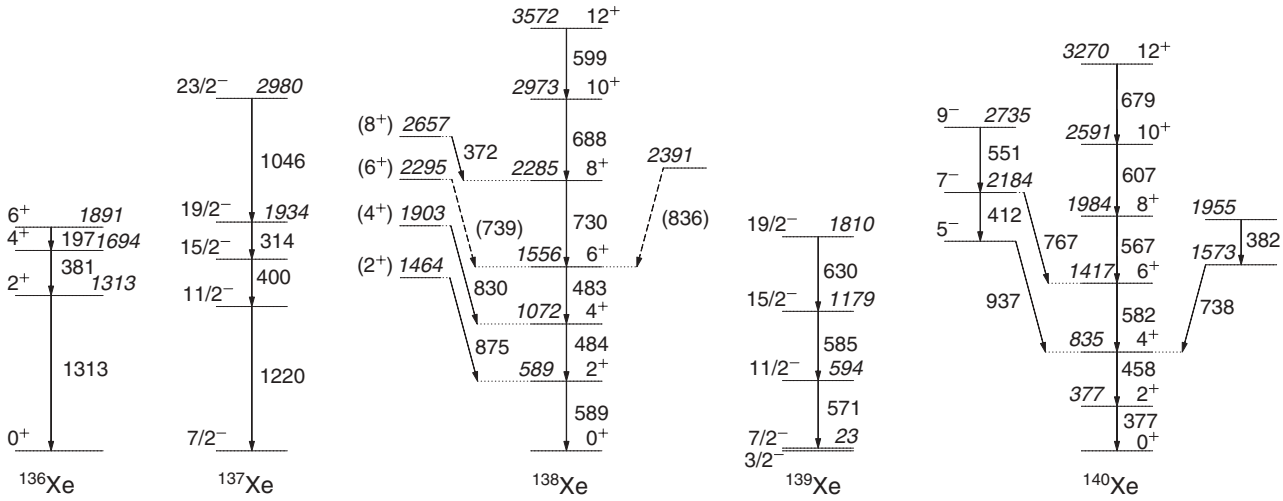

FIG. 11. Partial level schemes of Xe isotopes, as deduced from the present data set following coincidence analysis. The spins and parities of the levels have been adopted from earlier published works.

from this level to the 3.126-MeV level ($I = 8^+$) were not observed.

In ^{94}Sr, we could see up to the excitation energy $E_x = 3.923$ MeV ($I = 7^-\hbar$) (Fig. 10). In the present data set, we did not see the 1577 keV line, which was reported by Hamilton *et al.* [37]. Our results agree with Rząca-Urban *et al.* [33] to their suggestion that this line, proposed as the strongest coincident line with 837 keV by Jung *et al.* [38], might actually come from the β decay of ^{94}Rb. The agreement comes from the fact that we could not see it in coincidence with the 837 keV using a γ-γ matrix constructed with a narrow time window, nor it was visible while gating on the transition of its fragment partner. Naturally, we do not observe the 374 keV line which feeds the 2414-keV level, and hence, we do not confirm the existence of the 2788-keV level reported by Hamilton *et al.* [37]. The 458-keV transition that depopulates the 2604-keV level (4^-) and feeds in to the 2146 keV level (4^+) was seen in our data when gates were put on the 837-keV and/or the 1309-keV transition. However, we cannot confirm its occurrence in ^{94}Sr due to the fact that this 458-keV transition exists in its complementary fragment ^{140}Xe ($4^+ \rightarrow 2^+$) and the first excited state to ground state transition in ^{140}Xe, namely 377 keV, was also clear in the same gated spectrum.

Among the complementary fission fragments of Sr isotopes, ^{138}Xe was found to be the best populated nucleus. We could see up to spin $I = 12^+\hbar$ ($E_x = 3.572$ MeV) in its yrast band very clearly (Fig. 11). The latest experimental work on ^{138}Xe was reported by Korgul *et al.* [20], where the yrast sequence was extended up to 5.8 MeV in addition to the first observation of two non-yrast side bands. In the present data set, we can see the first few levels that constitute the proposed [20] γ vibration band. We confirm the non-yrast levels at 1464, 1903, and 2657 keV in the proposed γ vibration band through the observations of 875, 830, and 372-keV inter-band transitions, respectively. The other non-yrast band, which was speculated in the same work as resulting from coupling octupole excitation to the yrast cascade, was not seen in our data. Although we could see a strong 836-keV transition when gates were put on 589, 484, and 483 keV, the non-yrast level at 2391 keV could not be confirmed because 837 keV is a strong transition ($2^+ \rightarrow 0^+$) in one of its fragment partners, namely, ^{94}Sr ($4n$ evaporation).

Among other even-A Xe isotopes, we could see ^{136}Xe and ^{140}Xe in our data (Fig. 11). Like ^{138}Xe, we could see up to $I = 12^+\hbar$ ($E_x = 3.270$ MeV) in the yrast sequence of ^{140}Xe. This ^{140}Xe happens to be the only nucleus among the Xe isotopes where we could see the first few levels of the octupole band, proposed and observed by Bentaleb *et al.* [18] and also by Urban *et al.* [39]. It is to be noted that this is the first observation of an octupole band in any Xe isotope from the thermal neutron induced fission of ^{235}U data. Also, given the limited amount of data that were collected in comparison to the previous data sets, it might be possible to see this octupole band beyond (if it exists) whatever has been reported to date, and do a comprehensive study. In this context, the 258.4-keV ($5^- \rightarrow 3^-$) and 1136.4-keV ($3^- \rightarrow 2^+$) transitions, observed by Urban *et al.* [39], were not seen in our data. Therefore, the 3^- level ($E_x = 1513$ keV) of the octupole band under discussion could not be confirmed.

B. Kr and its complementary fragment Ba

While we looked at the Kr–Ba complementary fragment pair, we could see a well-populated ^{90}Kr (Fig. 12) nucleus. Along with that, a good number of well-populated Ba isotopes (^{140}Ba to ^{146}Ba) were also observed (Fig. 13) in the present data set. In fact, from our analysis of several complementary charge pairs, it has become evident that the Ba chain of isotopes is the largest that is observed in the thermal neutron induced fission of ^{235}U.

The latest work on ^{90}Kr was reported by Li *et al.* [40]. In its level scheme, we could see up to the excitation energy of $E_x = 3.895$ MeV in the yrast band, and along with that, a few other previously observed near-yrast transitions. The candidate level for a possible octupole band at $E_x = 1.506$ MeV, which depopulates in to the yrast

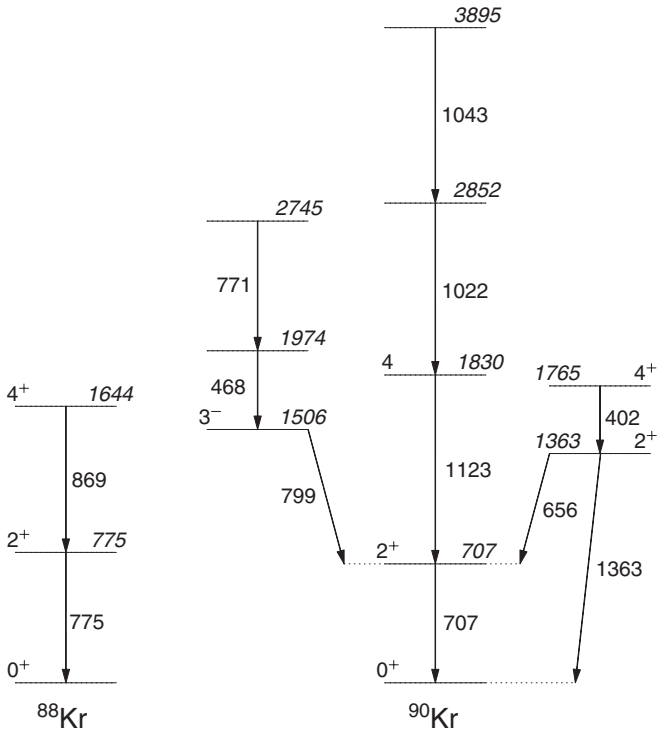

FIG. 12. Partial level schemes of Kr isotopes, as deduced from the present data set following coincidence analysis. The spins and parities of the levels have been adopted from earlier published works.

band at $I = 2^+$, was observed in our data. The 468- and 771-keV transitions, which are possible band members of this proposed octupole band, were also confirmed. However, the 1057-keV decay branch from the $I = 4^+$ level (to $I = 2^+$, $E_x = 0.707$ MeV level), proposed by Rząca-Urban *et al.* [41], was not observed in the present data set, although we could see every other transition leading to this level from the ground state of this nucleus. The relative intensities of strong transitions, depopulating yrast and near-yrast levels, are reported for the first time in Table IV.

In ^{144}Ba, we could see up to spin $I = 10^+\hbar$ ($E_x = 2.043$ MeV) in the yrast band (Fig. 13). Along with this, we could see the 7^- ($E_x = 1.355$ MeV), 9^- ($E_x = 1.772$ MeV), and 11^- ($E_x = 2.278$ MeV) levels of the octupole band in this nucleus. Though the interband (from the octupole band to the yrast band) $E1$ transitions, namely, 394 keV ($7^- \rightarrow 6^+$) and 302 keV ($9^- \rightarrow 8^+$), were vividly seen in our data, the $E1$ transitions from the yrast band to the octupole band which were seen in both the ^{252}Cf [42] and ^{248}Cm [14] data sets were elusive here, possibly because of their low intensities.

In ^{142}Ba, transitions up to $I = 10^+\hbar$ ($E_x = 2.926$ MeV) in its yrast sequence were seen clearly. We do not see the 602-keV transition from the 3346-keV level in the yrast band as proposed by Zhu *et al.* [17]. Instead, we agree with the work by Urban *et al.* that the excitation energy of the 10^+ level in the yrast band is 2.926 MeV [14] and that the transition 768 keV feeds the level at 2158 keV directly. In that same work [14], the transition 722 keV was assigned to the yrast band, and 641 keV was considered as an interband transition (from the 3795-keV yrast level to the 3154-keV level of the octupole band). These two transitions were earlier placed in the octupole band [17]. The assignments remain very much ambiguous as the yrast level at 3795 keV was reported as tentative [14]. A data set with good statistics out of the thermal neutron induced fission of ^{235}U might be of help to resolve the ambiguity between these two previous works. In the yrast sequence of ^{146}Ba, we could see up to $I = 8^+\hbar$ ($E_x = 1.483$ MeV). The octupole band [14] was also observed up to spin $I = 9^-\hbar$ ($E_x = 1.778$ MeV) along with the two strong interband $E1$ transitions, namely, 308 keV ($3^- \rightarrow 4^+$) and 511 keV ($5^- \rightarrow 4^+$).

Among the odd-A neutron-rich Ba isotopes, ^{143}Ba and ^{145}Ba were seen to be good prospects for a detailed investigation using the thermal neutron induced fission of ^{235}U. Yrast states up to spin $I = \frac{21}{2}^-\hbar$ ($E_x = 1.580$ MeV) and spin $I = \frac{11}{2}^-\hbar$ ($E_x = 0.463$ MeV) were seen in ^{143}Ba and ^{145}Ba, respectively. The first few levels of the octupole bands [43] in these two nuclei were also seen even with this limited data set. Among other near yrast levels in ^{143}Ba, we could see the level at $E_x = 1.525$ MeV ($I = \frac{17}{2}^+$). In ^{145}Ba, a new band with rigid body moment of inertia was reported by Zhu *et al.* [43]. It was conjectured as the first example of a pairing-free structure in neutron-rich nuclei or a type of superdeformed band. Further study with a different data set is needed to confirm these proposed structures.

C. Zr and its complementary fragment Te

The level schemes of Zr isotopes as obtained in the present measurement are shown in Fig. 14. In ^{98}Zr, we could see up

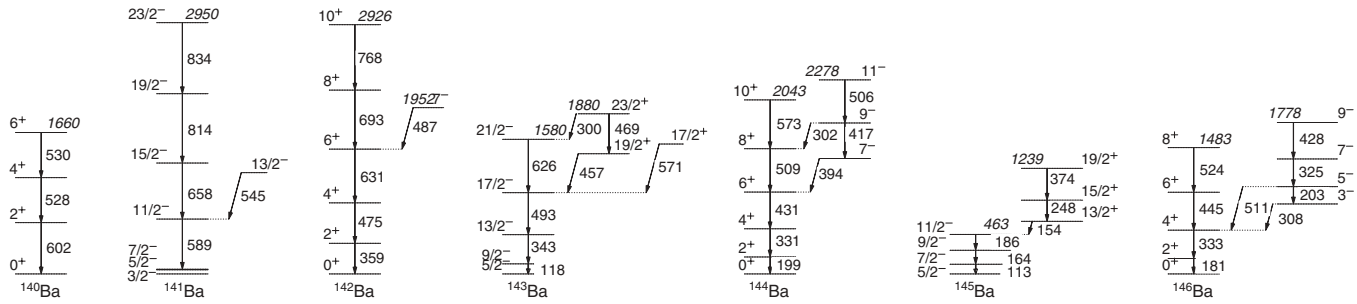

FIG. 13. Partial level schemes of Ba isotopes, as deduced from the present data set following coincidence analysis. The spins and parities of the levels have been adopted from earlier published works.

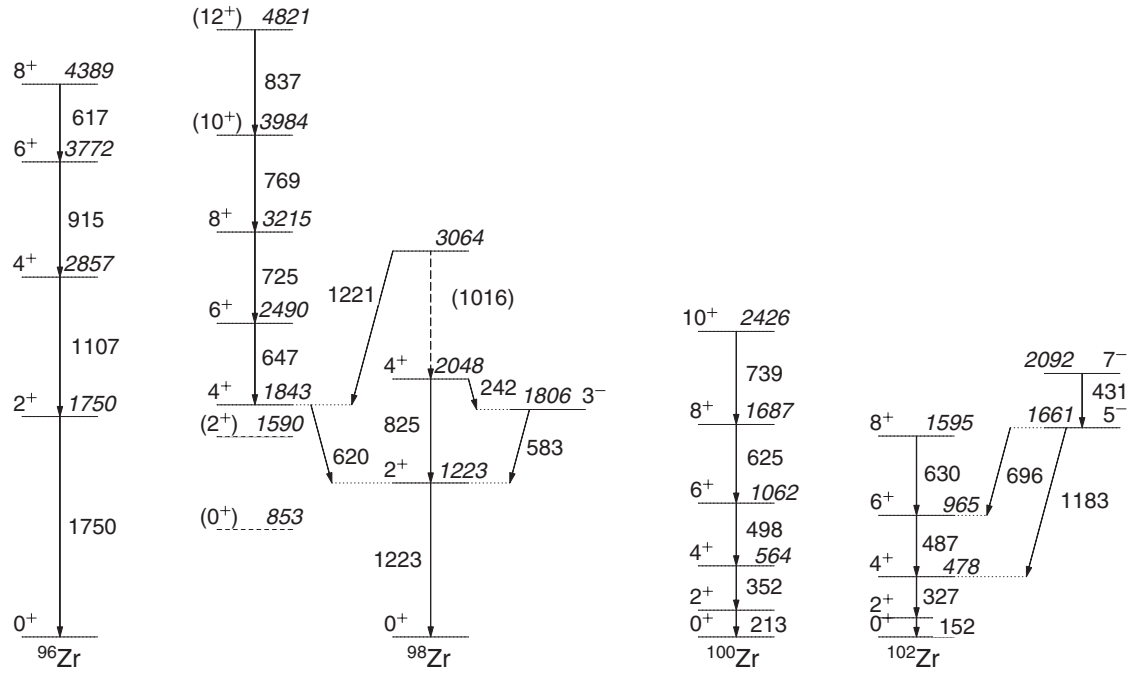

FIG. 14. Partial level schemes of Zr isotopes, as deduced from the present data set following coincidence analysis. The spins and parities of the levels have been adopted from earlier published works.

to an excitation energy of $E_x = 4.821$ MeV [$I = (12^+)\ \hbar$] in its yrast band. Although we could not see the 0_2^+ and 2_2^+ states as observed earlier [44,45] (included in the level scheme in Fig. 14 to assist visualization of their placement), we did notice some notable discrepancies (and similarities) in the quasivibrational structure built on 0_2^+ with respect to previous studies. Our data agree well with the work of Urban *et al.* [34], where it was reported that there is only one 769-keV transition in this band, and that the 837-keV (neither 835 [37] nor 834 keV [36]) γ line feeds directly to the 3984-keV [$I = (10^+)\ \hbar$] level. So we doubt the existence of the 4756.4-keV (or 4755 keV) and the 3986.4-keV (or 3985.1 keV) levels as reported in previous work [36,37]. Also, like all other previous SF data, we can neither see the 0_3^+ level nor the strongly deformed band built on it as suggested previously [44,45].

The ground state band in ^{100}Zr was observed up to an excitation energy of $E_x = 2.426$ MeV ($I = 10^+\hbar$) in the present data set (Fig. 14). This nucleus exhibits a clear coexistence of a near-spherical band (built on a 331.1-keV state) and ground band with a well-deformed prolate shape [46]. In the latest high-spin work on this nucleus by Hwang *et al.* [47], this near-spherical excited band in ^{100}Zr was extended from 4^+ up to 12^+, and it was proposed that this 12^+ happens to be the highest spin to which a coexisting near-spherical band was observed in the $A \sim 100$ mass region. Although the low- and medium-spin states were well populated in most of the nuclei in this mass region in the present data set, we could not observe even the first few transitions of this band. This could be attributed to the lesser statistics, and it could be suggested that this near-spherical excited band is very weak in intensity compared to the ground band.

The nucleus ^{102}Zr was observed up to $E_x = 1.595$ MeV ($I = 8^+\hbar$) in its yrast sequence (Fig. 14) in the present data set. The first two levels of the $K^\pi = 5^-$ band, which couples to the ground state band very strongly, were seen clearly, although the other high-spin band members of this band were elusive. The new set of coincident γ transitions (speculated as the transitions for the unnatural parity partner states of the $K^\pi = 5^-$ band) that was observed in the ^{238}U(α, f) reaction [48] was not seen in our data obtained from the thermal neutron induced fission of ^{235}U.

The level schemes of Te isotopes as obtained in the present investigation are shown in Fig. 15. Among all the Te isotopes that were observed in the present data set, ^{134}Te seems to be the highest populated nucleus. The latest work on this nucleus was reported by Saha *et al.* [49], where a new level was observed at 2683 keV in its $\pi g_{7/2}d_{5/2}$ multiplet. This level was reported as the missing 3^+ member of this multiplet, which depopulates into the 1279-keV 2^+ level by a strong 1404-keV transition [49]. Surprisingly, apart from the 2727-keV 5^+ level, which feeds into the 2397-keV 6_2^+ level by a 330-keV transition, we could not see any other member level of this multiplet out of the present data set. Above the 164-ns 6_1^+ isomeric level, the high-energy 2322-keV ($9^- \rightarrow 6^+$) transition was observed apart from the 706 and 330-keV γ rays. The levels that involve a possible core excitation [49] remain elusive in this data set, possibly due to poor statistics.

The latest work on ^{136}Te by Korgul *et al.* [20] extended the yrast cascade up to 5.1 MeV. We could see up to $E_x = 2.8$ MeV ($I = 10^+\hbar$) very clearly (Fig. 15) in our data set. The 395-keV transition ($12^+ \rightarrow 10^+$), which was observed by

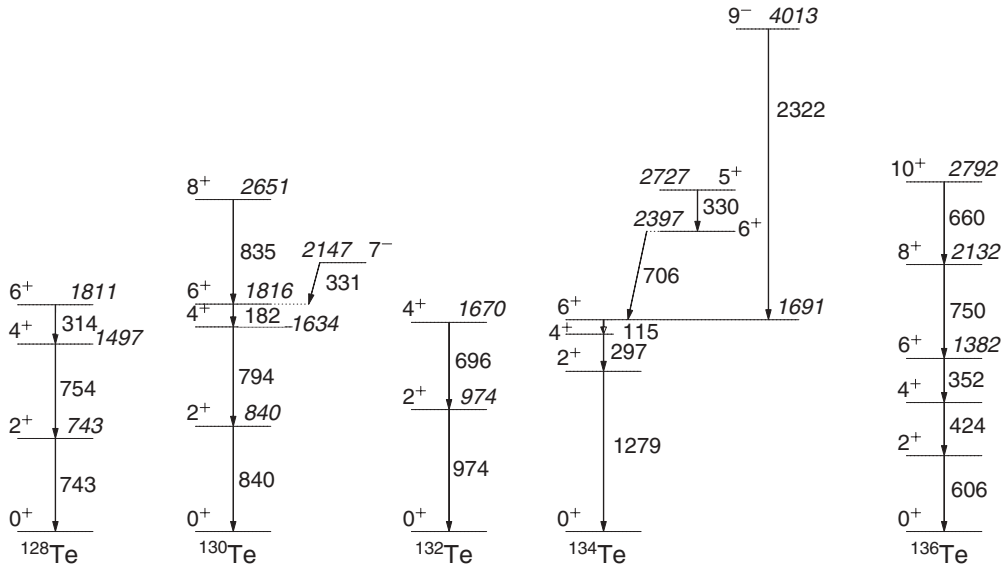

FIG. 15. Partial level schemes of Te isotopes, as deduced from the present data set following coincidence analysis. The spins and parities of the levels have been adopted from earlier published works.

Korgul *et al.* [20] and was proposed as having comparable intensity with respect to the lower-lying known transitions, was not observed even after summing all possible gates. This observation calls for further investigation in its high-spin states using a different reaction.

Our efforts to see and confirm the $(\nu h_{11/2})^2$ 10^+ isomeric level in ^{130}Te in the present data set did not succeed though we observed well up to $E_x = 2.651$ MeV ($I = 8^+\hbar$) below this microsecond isomeric level (Fig. 15). The latest work on this nucleus by Broda *et al.* [23] reported this isomeric level to be at $E_x = 2667$ keV, which decays to the 2648-keV ($I = 8^+\hbar$) level by an unobserved 19-keV γ transition. Due to the clear observations of the 835-keV ($8^+ \rightarrow 6^+$ transition, reported as 833 keV in Ref. [23]) and 840-keV ($2^+ \rightarrow 0^+$ transition, reported as 839 keV in Ref. [23] and as 840 keV in Ref. [24]) transitions, it seems that the proposed 19-keV γ ray will have slightly less energy (-3 keV) if it really exists. The highly retarded $E1$ transition of energy 331 keV ($7^- \rightarrow 6^+$) was clearly seen similar to all other previous work. The occurrence of another low-energy $E2$ transition of energy 46 keV, connecting the 7^- ($E_x = 2.147$ MeV) and 5^- ($E_x = 2.101$ MeV) states, was deduced in one of the previous works, where the ^{64}Ni + ^{130}Te deep-inelastic reaction was used [24]. However, the data out of ^{136}Xe + ^{232}Th Gammasphere experiment could not confirm the 468-keV ($5^- \rightarrow 4^+$) transition, and thereby the existence of the 2.101 MeV ($I = 5^-$) level [23]. The present study using the data from thermal neutron induced fission of ^{235}U remains consistent with the Gammasphere measurement.

VII. SUMMARY

The online measurement of coincident γ rays from neutron-rich fission fragment nuclei is attempted for the first time in the case of thermal neutron induced fission of ^{235}U. The relative isotopic yield distributions of several isotopes of six elements were measured using the prompt γ-γ coincidence technique. The distribution parameters are found to agree reasonably well with the numbers extracted from the data in the literature. The rates of Ba and Sr isotopes in coincidence with a complementary fragment nucleus are presented for the first time. It is observed that in the case of the Xe–Sr fragment pair, the 3-neutron evaporation channel dominates, whereas, in the case of the Ba–Kr fragment pair, the 2-neutron evaporation channel is the maximum. The average angular momenta of the fission fragment nuclei were estimated from the relative intensities of the transitions in the ground band cascade. It is interesting to note that the average angular momenta of the lighter and the heavier fission fragment nuclei are distinctly different, but they approach each other as the symmetric division is approached. A systematic study of the yrast and near-yrast level structures of the neutron-rich nuclei produced in this reaction was performed. The level sequences are compared with the previously reported works that used different reactions or SF data. The relative intensities of yrast and near-yrast transitions were measured and compared with these previous works. Employing this novel technique of prompt γ-γ coincidence in thermal neutron induced fission of ^{235}U, a detailed spectroscopic study of the neutron-rich fission fragment nuclei can be performed with a larger detector array.

ACKNOWLEDGMENTS

The authors would like to thank Dr. S. S. Kapoor and Dr. S. Kailas for their constant support and encouragement to this work. The help and cooperation of the CIRUS reactor staff during the experiment is gratefully acknowledged. Thanks are due to A. K. Sahu, A. L. Inkar, and R. V. Jangle for their help during the experiment. The authors are also thankful to Metallic Fuels Division, BARC, for providing the UAl_3 target.

[1] Peter Möller and A. Iwamoto, Phys. Rev. C **61**, 047602 (2000).
[2] U. Brosa, S. Grossmann, and A. Müller, Phys. Rep. **197**, 167 (1990).
[3] J. Benlliure, A. Grewe, M. de Jong, K.-H. Schmidt, and S. Zhdanov, Nucl. Phys. A **628**, 458 (1998).
[4] P. A. Butler and W. Nazarewicz, Nucl. Phys. A **533**, 249 (1991).
[5] L. Satpathy and S. K. Patra, J. Phys. G **30**, 771 (2004).
[6] L. S. Danu *et al*., Phys. Rev. C **81**, 014311 (2010).
[7] G. M. Ter-Akopian *et al*., Phys. Rev. Lett. **77**, 32 (1996).
[8] D. C. Biswas *et al*., Eur. Phys. J. A **7**, 189 (2000).
[9] R. Vandenbosch and J. Huizenga, *Nuclear Fission* (Academic Press, New York, 1996).
[10] T. Friedrichs, Ph.D. Thesis, Technischen Universität Carolo-Wilhelmina, Braunschweig, 1998.
[11] D. Rochman, H. Faust, I. Tsekhanovich, F. Gönnenwein, F. Storrer, S. Oberstedt, and V. Sokolov, Nucl. Phys. A **710**, 3 (2002).
[12] A. Bail, O. Serot, L. Mathieu, O. Litaize, T. Materna, U. Köster, H. Faust, A. Letourneau, and S. Panebianco, Phys. Rev. C **84**, 034605 (2011).
[13] G. M. Ter-Akopian *et al*., Phys. Rev. Lett. **73**, 1477 (1994).
[14] W. Urban *et al*., Nucl. Phys. A **613**, 107 (1997).
[15] J. H. Hamilton *et al*., Prog. Part. Nucl. Phys. **38**, 273 (1997).
[16] J. H. Hamilton *et al*., Phys. Rep. **264**, 215 (1996).
[17] S. J. Zhu *et al*., Phys. Lett. B **357**, 273 (1995).
[18] M. Bentaleb *et al*., Z. Phys. A **354**, 143 (1996).
[19] W. Urban *et al*., Z. Phys. A **358**, 145 (1997).
[20] A. Korgul *et al*., Eur. Phys. J. A **7**, 167 (2000).
[21] M.-G. Porquet *et al*., Eur. Phys. J. A **28**, 153 (2006).
[22] D. Pantelica *et al*., Phys. Rev. C **72**, 024304 (2005).
[23] R. Broda, B. Fornal, W. Królas, T. Pawlat, J. Wrzesiński, D. Bazzacco, G. de Angelis, S. Lunardi, and C. Rossi Alvarez, Eur. Phys. J. A **20**, 145 (2004).
[24] C. T. Zhang *et al*., Nucl. Phys. A **628**, 386 (1998).
[25] T. A. Khan, D. Hofmann, and F. Horsch, Nucl. Phys. A **205**, 488 (1973).
[26] D. C. Biswas *et al*., Proc. DAE Symp. on Nucl. Phys. **55**, 670 (2010).
[27] D. C. Radford, Nucl. Instrum. Methods Phys. Res., Sect. A **361**, 297 (1995).
[28] http://radware.phy.ornl.gov/.
[29] A. C. Wahl *et al*., At. Data Nucl. Data Tables **39**, 1 (1988).
[30] J. B. Wilhelmy, E. Cheifetz, R. C. Jared, S. G. Thompsom, and H. R. Bowman, Phys. Rev. C **5**, 2041 (1972).
[31] J. K. Hwang *et al*., Phys. Rev. C **69**, 067302 (2004).
[32] *Table of Isotopes*, 8th ed. edited by R. B. Firestone and V. S. Shirley (John Wiley and Sons, New York, 1996).
[33] T. Rząca-Urban *et al*., Phys. Rev. C **79**, 024319 (2009).
[34] W. Urban *et al*., Nucl. Phys. A **689**, 605 (2001).
[35] L. K. Peker, Nucl. Data Sheets **68**, 165 (1993).
[36] C. Y. Wu *et al*., Phys. Rev. C **70**, 064312 (2004).
[37] J. H. Hamilton, A. V. Ramayya, S. J. Zhu, G. M. Ter-Akopian, Yu. Ts. Oganessian, J. D. Cole, J. O. Rasmussen, and M. A. Stoyer, Prog. Part. Nucl. Phys. **35**, 635 (1995).
[38] G. Jung, B. Pfeiffer, L. J. Alquist, H. Wollnik, P. Hungerford, S. M. Scott, and W. D. Hamilton, Phys. Rev. C **22**, 252 (1980).
[39] W. Urban, T. Rząca-Urban, N. Schulz, J. L. Durell, W. R. Phillips, A. G. Smith, B. J. Varley, and I. Ahmed, Eur. Phys. J. A **16**, 303 (2003).
[40] K. Li *et al*., Int. J. Mod. Phys. E **20**, 1825 (2011).
[41] T. Rząca-Urban *et al*., Eur. Phys. J. A **9**, 165 (2000).
[42] W. R. Phillips, I. Ahmad, H. Emling, R. Holzmann, R. V. F. Janssens, T.-L. Khoo, and M. W. Drigert, Phys. Rev. Lett. **57**, 3257 (1986).
[43] S. J. Zhu *et al*., Phys. Rev. C **60**, R051304 (1999).
[44] G. Lhersonneau *et al*., Phys. Rev. C **49**, 1379 (1994).
[45] K. Kawade, G. Battistuzzi, H. Lawin, H. A. Selič, K. Sistemich, F. Schussler, E. Monnand, J. A. Pinston, B. Pfeiffer, and G. Jung, Z. Phys. A **304**, 293 (1982).
[46] S. Raman *et al*., At. Data Nucl. Data Tables **36**, 1 (1987).
[47] J. K. Hwang *et al*., Phys. Rev. C **74**, 017303 (2006).
[48] H. Hua, C. Y. Wu, D. Cline, A. B. Hayes, R. Teng, R. M. Clark, P. Fallon, A. Goergen, A. O. Macchiavelli, and K. Vetter, Phys. Rev. C **69**, 014317 (2004).
[49] S. K. Saha *et al*., Phys. Rev. C **65**, 017302 (2001).
[50] K. Li *et al*., Phys. Rev. C **78**, 044317 (2008).
[51] J. A. Cizewski *et al*., Phys. Rev. C **47**, 1294 (1993).
[52] P. J. Daly *et al*., Phys. Rev. C **59**, 3066 (1999).